Kinetics and Mechanism of Morphological Transition from Lamella to Cylinder Microdomain in Polystyrene-*block*-poly(ethylene-*co*-but-1-ene)-*block*-polystyrene Triblock Copolymer

Unyong Jeong, Hee Hyun Lee, H. Yang, and Jin Kon Kim*

Department of Chemical Engineering and Polymer Research Institute, Electronic and Computer Engineering Divisions, Pohang University of Science and Technology, Pohang, Kyungbuk 790-784, Korea

Shigeru Okamoto

Department of Material Science & Engineering, Nagoya Institute of Technology, Gokiso-cho, Showa-ku, Nagoya 466-8555, Japan

Sakae Aida and Shinichi Sakurai*

Department of Polymer Science & Engineering, Kyoto Institute of Technology, Sakyo-ku, Kyoto 606-8585, Japan

Received August 22, 2002

ABSTRACT: The kinetics and mechanism of morphological transition from nonequilibrium lamella to cylinder microdomain in a polystyrene-*block*-poly(ethylene-*co*-but-1-ene)-*block*-polystyrene (SEBS) triblock copolymer were studied by using time-resolved synchrotron small-angle X-ray scattering (SAXS), transmission electron microscopy (TEM), and rheology. The sample cast from toluene solution formed a nonequilibrium morphology of the alternating lamellae (LAM) of polystyrene (PS) and poly(ethylene-*co*-but-1-ene) (PEB) blocks because toluene is a good solvent for PS chains but a poor solvent for PEB chains. LAM of PS and PEB blocks was transformed into the hexagonally close packing (HEX) of PS cylinders in PEB matrix when the as-cast sample was annealed above 140 °C, which is above the glass transition temperature of the PS block. From the time-resolved SAXS and TEM, the coexistence of the LAM and HEX microdomains was clearly confirmed during the entire process of the order-to-order transition (OOT) from LAM to HEX, and the lamellar fraction in the coexisting phase decreased with increase of the annealing time. It was also found that the storage modulus during the transition linearly decreased with the lamellar fraction. The temporal change in the LAM fraction in the coexisting phase was fitted by the Avrami-type exponential decay function. The mechanism of the OOT was discussed on the basis of the evaluated Avrami exponent (n). We found that the value of n was ∼1 at higher annealing temperatures (above 160 °C), whereas it was ∼0.5 at lower annealing temperatures. Thus, it is concluded that at higher temperatures the nucleation and growth of the HEX microdomains from LAM phase result from both interlayer correlation of the modulation and in-layer modulation of LAM layers (2-dimensional growth). On the other hand, at lower temperatures, one-dimensional growth from the in-layer modulation induced the nucleation and growth of HEX microdomains.

I. Introduction

Block copolymers form regularly ordered microdomain structures at the thermodynamic equilibrium state because of the repulsive energetic interaction between constituent block chains.[1−4] It is well-known that those microdomain structures are spheres arranged in a body-centered-cubic lattice, cylinders in a hexagonal lattice, double gyroid, or alternating lamellae depending upon the composition, molecular weight, and temperature.[2−4] The control of morphologies of a block copolymer is important, since mechanical properties of the block copolymer strongly depend on their morphologies.[5] Many experimental and theoretical studies have been performed on phase behavior of block copolymers.[6−35]

Phase transitions between ordered microdomain structures, so-called order-to-order transition (OOT), have attracted much attention both theoretically[6−11] and experimentally.[12−35] It is known that the design of block copolymers with OOT needs a judicious choice of block composition and total molecular weight of block copolymer.[17−35] Contrary to experiments on the OOT in equilibrium morphologies, nonequilibrium morphologies can provide an alternative method to study the OOT. This is because a nonequilibrium morphology can be easily formed when block copolymers are cast from solution with a selective solvent.[14,29]

One of us studied the kinetics of OOT from nonequilibrium polybutadiene (PB) cylinders to equilibrium lamellae in polystyrene-*block*-polybutadiene-*block*-polystyrene (SBS) triblock copolymers.[14] It is of interest to study whether the kinetics of OOT from nonequilibrium lamellae to equilibrium cylinders is described by the same mechanism of the above. In the present paper, we report on the kinetics of OOT from nonequilibrium lamellae to equilibrium PS cylinders in a polystyrene-*block*-poly(ethylene-*co*-but-1-ene)-*block*-polystyrene (SEBS) triblock copolymer. The apparent activation energies and the Avrami exponents for the OOT were evaluated in order to discuss the mechanism of the OOT. Furthermore, the rheological change during the OOT was monitored and compared with SAXS results.

* To whom correspondence should be addressed. E-mail: jkkim@postech.ac.kr and shin@ipc.kit.ac.jp.

10.1021/ma021376v CCC: $25.00
Published on Web 02/13/2003

II. Experimental Section

The sample used in this study was an SEBS triblock copolymer [Kraton G1652; Shell Development Co.]. The number-average molecular weight, M_n, the heterogeneity index for molecular weight distribution, M_w/M_n, and the volume fraction of polystyrene (PS), ϕ_{PS}, were determined to be 5.4×10^4, 1.10, and 0.227, which are measured by membrane osmometry, gel permeation chromatography, and ^{1}H nuclear magnetic resonance spectroscopy (NMR), respectively. The average number of ethyl side group on the poly(ethylene-*co*-but-1-ene) (PEB) block chain was determined by ^{13}C NMR to be 71 per 1000 carbon atoms in the PEB block chain. From this value the microstructure in the original PB before hydrogenation is estimated to be 25 and 75 mol % for 1,2- and 1,4-linkages, respectively. The film samples subjected to the SAXS measurements were prepared by solution-casting at room temperature using toluene, which is a selective solvent for PS block.[36]

The SAXS measurements with synchrotron radiations were conducted at the 4C1 beam line in the Pohang Light Source (PLS), Korea. The primary beam was monochromatized with double Si(111) crystals at the wavelength of 0.1598 nm, and then it was focused on a detector plane by a bent cylindrical mirror. A one-dimensional position-sensitive detector (Diode-Array PSD; Princeton Instruments Inc.; model ST-120) with the distance of each diode of 25 μm was used. Typical exposure time for G1652 samples with 1.2 mm thickness was 30 s. The sample was settled in such a way that the film normal was parallel to the incident beam trajectory (through view). The measured scattering intensities were corrected for air scattering, for absorption due to the sample, and further for the thermal diffuse scattering (TDS) arising from density fluctuations. Here, the scattering intensity of TDS was conventionally assumed to be that measured at the highest q region covered in this study ($1.2\ \text{nm}^{-1} < q < 1.5\ \text{nm}^{-1}$), where the scattering intensities reached an almost constant level, irrespective of the scattering angle.[14−16] The magnitude of the scattering vector (q) is given by

$$q = (4\pi/\lambda)\sin(\theta/2) \tag{1}$$

where λ is the wavelength of the X-ray and θ is the scattering angle.

For the study of the kinetics of the morphological transition, time-resolved SAXS measurements were performed upon temperature-jump (T-jump). A copper sample cell containing the sample preheated at 110 °C for 5 h was put into another cell holder maintained at specific temperatures (140, 150, 157, 162, and 168 °C), which were above the glass transition temperature of PS blocks ($T_{g,PS}$) of 89 °C measured by a differential scanning calorimeter (DSC 7 series, Perkin-Elmer) at a heating rate of 10 °C/min. The temperature was stabilized at a preset temperature within 1 min after the T-jump.

The temporal storage modulus, G', was measured by an Advanced Rheometrics Expanded System (ARES) after the specimen was jumped from 110 °C to a preset temperature. The strain amplitude (γ_0) and the frequency (ω) are 0.005 and 0.1 rad/s, respectively, which lie in a linear viscoelastic region.

The micodomain structures of the samples were examined by transmission electron microscopy (JEOL 1200EX) operated at 120 kV. Cryogenic ultrasectioning was performed with an RMC (MT-700) microtomer at −100 °C. Then, specimens were stained with RuO_4 for 30 min, which selectively stained the PS microdomains.

III. Results and Discussion

Figure 1 shows SAXS profiles [intensity ($I(q)$) vs q] for the samples with various thermal histories: (a) as-cast, (b) annealed at 110 °C for 300 min, (c) annealed at 120 °C for 120 min after annealing at 110 °C for 300 min, (d) annealed at 140 °C for 60 min after annealing at 110 °C for 300 min, and (e) annealed at 168 °C for 120 min after annealing at 110 °C for 300 min. Diffraction peaks of the as-cast sample are seen at the relative

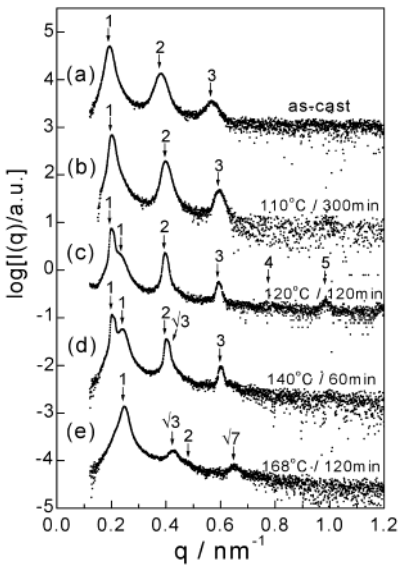

Figure 1. SAXS profiles of through view of the film for SEBS at various thermal histories: (a) as-cast; (b) annealed at 110 °C for 300 min; (c) annealed at 120 °C for 120 min after annealing at 110 °C for 300 min; (d) annealed at 140 °C for 60 min after annealing at 110 °C for 300 min; and (e) annealed at 168 °C for 120 min after annealing at 110 °C for 300 min. To avoid overlap, the SAXS profiles were shifted vertically.

q-positions of 1:2:3, reflecting well-ordered lamellar microdomains (LAM). Such nonequilibrium morphology in the casting solution is kinetically locked when the PS domains vitrify as the polymer concentration increases. Namely, the nonequilibrium morphology does not have a chance to transform into more stable HEX microdomains during the subsequent casting process where the remaining solvent was thoroughly evacuated. For a sample annealed at 110 °C, SAXS peaks were sharpened, but the first-order peak moved to slightly higher q (∼4% increase), indicating that LAM ordering was improved at 110 °C, and the transition to HEX did not occur at all at this temperature. The slightly increased q^* (or slightly decrease in d spacing) with annealing at 110 °C was due to the fact that the residual stress stored during the vitrification of PS block was relaxed at higher temperatures. In other words, vitrified PS chains can slowly relax at 110 °C, allowing better LAM perfection, but this temperature was still insufficient to achieve the transition to HEX due to the vicinity of $T_{g,PS}$.

On the other hand, for a sample annealed at 168 °C, three peaks appeared at q positions of $1{:}\sqrt{3}{:}\sqrt{7}$, typical of the scattering from hexagonally packed cylinders (HEX). This SAXS profile indicates thermally induced morphological transition from nonequilibrium LAM to equilibrium HEX upon annealing at 168 °C (far above $T_{g,PS}$). It is quite natural that G1652 with $\phi_{PS} = 0.227$ has HEX microdomains at equilibrium condition. The SAXS profiles (c) and (d) showed the double first-order peaks arising from LAM and HEX microdomains, suggesting that LAM and HEX phases coexist at these two annealing conditions.

To investigate in detail the double first-order peaks, we performed the T-jump from 110 °C to a preset temperature. Figure 2 shows typical examples of the change in the SAXS profiles with the annealing time at two temperatures (140 and 168 °C). For both T-jumps, a gradual disappearance of higher-order LAM peaks at the expense of the evolution of HEX peaks was

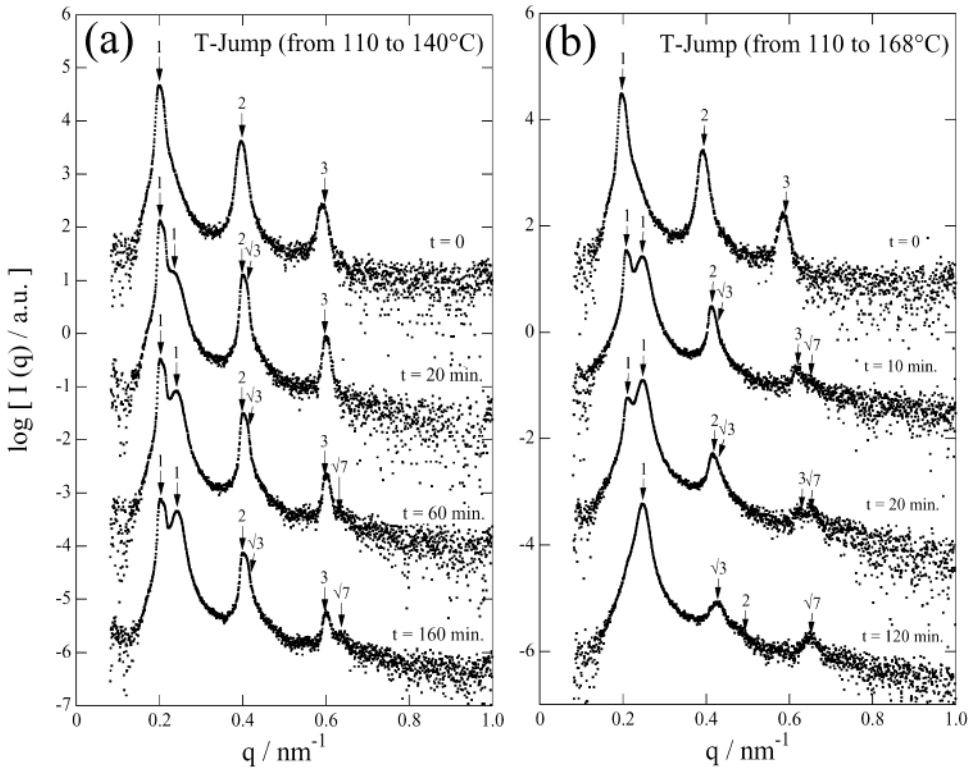

Figure 2. Changes in the SAXS profiles with the annealing time at two different T-jumps from 110 °C: (a) 140 °C; (b) 168 °C.

observed. This tendency was observed in all other T-jumps, although LAM peaks disappeared earlier with increasing T-jump temperature. For the T-jump to 168 °C, the LAM peaks completely disappeared at $t \geq 120$ min, whereas the LAM peaks were still dominant even at 160 min for the T-jump to 140 °C.

TEM images after T-jumps to 140 and 168 °C followed by annealing for 20 min are shown in Figure 3. It is seen in Figure 3a that HEX microdomains are clearly generated from LAM layers, although the area of HEX is small. The boundary between LAM and HEX phases was distinct. For the specimen annealed at 168 °C for 20 min, the HEX phase becomes dominant over the LAM phase, as shown in Figure 3b. Interestingly, the modulation and perforation of LAM, marked by the arrows in Figure 3b, are visible, even though the area corresponding to these regions was very small. However, this kind of the LAM modulation (ML) or perforation (PL) is barely seen in Figure 3a. This suggests that the transition mechanism of OOT from LAM to HEX at lower temperature (or shallow T-jump) is different from that at higher temperature (deep T-jump). This behavior will be complemented with different values of the Avrami exponent at two temperature regimes, which will be discussed later.

Very recently, Wang and Lodge[30] showed that the OOT from HEX to gyroid for a solution consisting of polystyrene-*block*-polyisoprene and dibutyl phthalate proceeds directly by a nucleation and growth for shallow quench, but a metastable intermediate structure of hexagonally perforated layer (HPL) was observed for deep quenches. Thus, TEM images given in Figure 3 might be consistent with the results given in ref 30, although the OOT in this study was the transition of kinetically frozen LAM to equilibrium HEX phase. However, we did not observe a clear evidence of ML or PL during the OOT from SAXS or rheology results. This indicates that even though this kind of intermediate state might exist during the OOT at higher annealing temperatures (deep T-jumps), it would be a short-lived intermediate, or the amount of this intermediate was small.

Of course, it cannot be completely excluded that SAXS profiles of ML (or PL) are not much different from LAM with random grains, and the difference in rheological properties between ML (or PL) and LAM is not large. The best way to test the existence of ML (or HPL) is to use shear-aligned LAM.[28] In ref 28, two intermediate structures (ML and HPL) were clearly observed between LAM and HEX. According to Wang and Lodge,[30] the transition mechanism between HEX and Gyroid for aligned sample is similar to unaligned sample. Thus, we tried to perform macroscopically shear alignment using a large-amplitude oscillatory shearing (LAOS) with $\omega = 0.08$ rad/s and $\gamma_0 = 50\%$ for specimen with 1.2 mm thickness and 50 mm diameter. However, we found via 2-D SAXS experiment that LAM did not align even under LAOS at 110 °C for 4 h. This is attributed to the fact that the temperature was close to the T_g of PS block. In the meantime, when a specimen was aligned under LAOS at 140 °C for 1 h, we found, via 2-D SAXS, that both HEX cylinders and LAM layers were well-aligned toward the flow direction (x-direction). However, we barely saw any scattering peaks or TEM images corresponding to HPL (or ML or PL) for this aligned sample. Namely, both 6-fold diffraction spots in q_x-q_z (shear plane) and four additional weak spots in q_x-q_y plane, corresponding to the characteristics of HPL,[28] were not observed.

Hajduk et al.[29] showed that, during OOT from kinetically frozen state of LAM to equilibrium HEX, there exists an intermediate state of ML, and this ML would be a long-lived or pseudo-equilibrium state. Interestingly, they employed PS−PEB diblock copolymer cast from tetrahydrofuran (THF), which is a selective solvent to PS block. They also showed that this ML was detected

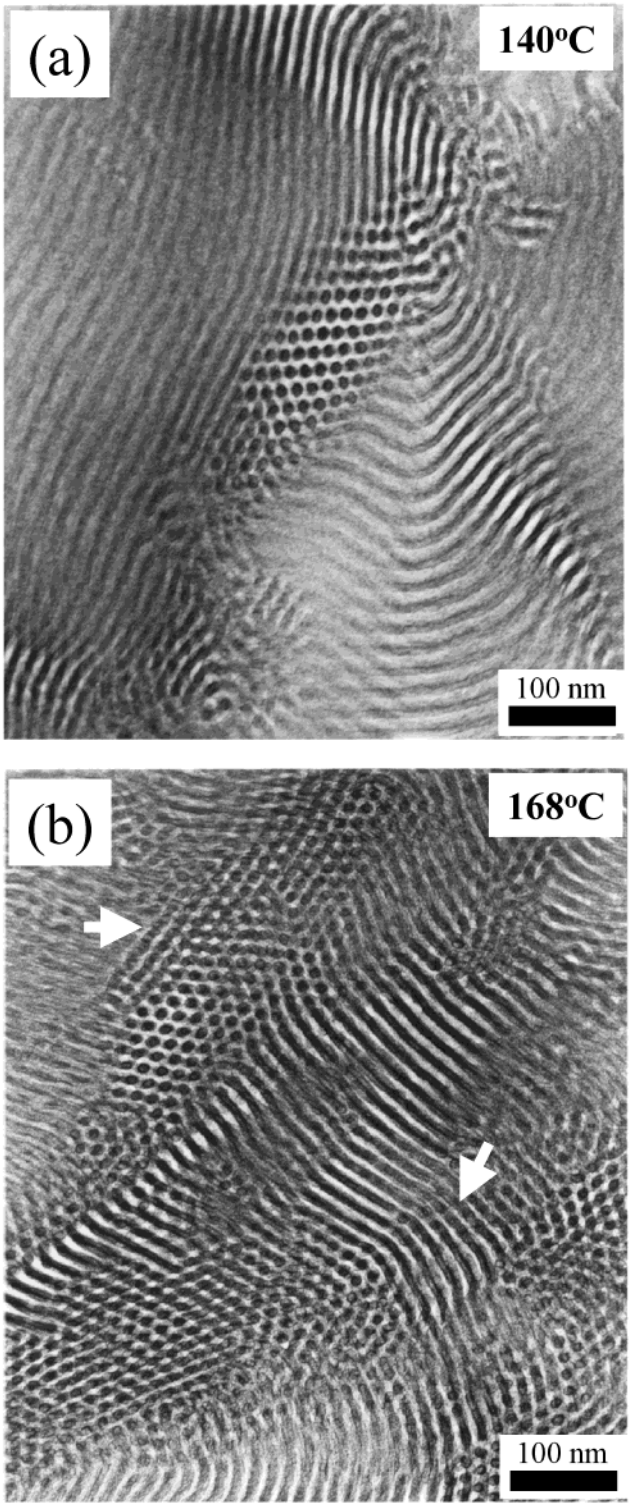

Figure 3. TEM images after two T-jumps ((a) 140 °C; (b) 168 °C) followed by annealing for 20 min. Before T-jumps, specimens were annealed at 110 °C for 5 h.

after the sample was cooled from equilibrium HEX state. These results imply that the stability of the intermediate state depends on volume fraction of PS block. The volume fractions of the minor block studied in refs 28, 29, and 30 are 0.35, 0.29, and 0.30, respectively, which are larger than that (0.23) of SEBS investigated here. This indicates that the stability of ML for a block copolymer with higher amount of the minor block might be better than that with lower amount.

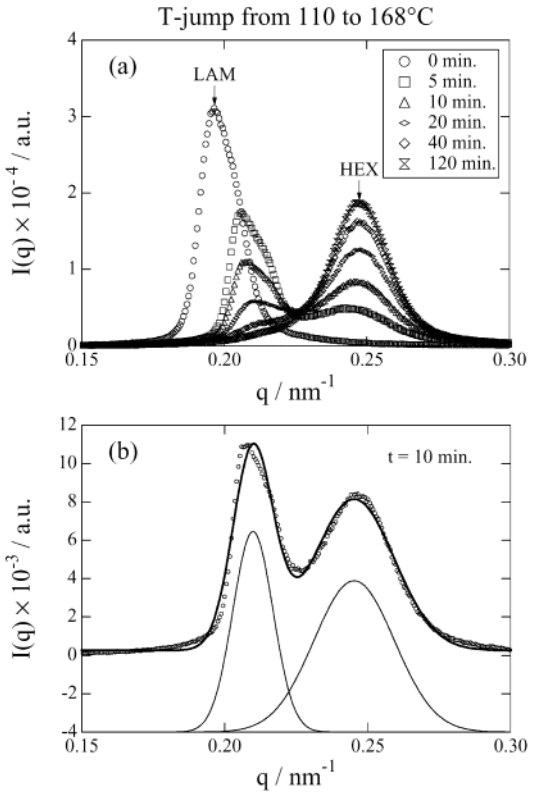

Figure 4. (a) Temporal changes in SAXS profiles for the T-jump to 168 °C, where the scattering intensity $I(q)$ is plotted against q in the range $0.15 \leq q \leq 0.30$ nm^{-1} covering the double first-order peaks. (b) An example of the computational peak decomposition for $t = 10$ min by using eq 2. The decomposed peaks are shown as dotted curves.

Furthermore, we did not observe any evidence of ML or PL in SAXS and TEM, when the specimen was cooled from equilibrium HEX. Therefore, we conclude that LAM and HEX phases coexisted during the entire process of this OOT, and that even though an intermediate ML or PL might be formed at higher T-jumps, the amount would be very small or it would be short-lived.

To estimate the conversion (or the amount) of HEX phase from LAM, SAXS profiles in Figure 2b were expanded in Figure 4a, where $I(q)$ in the range $0.15 \leq q \leq 0.30$ nm^{-1} for the double first-order peaks are highlighted. These peaks are easily decomposed by using a mathematical expression comprising Gaussian peak function

$$I(q) = \sum_i \left\{ \frac{A_i}{\sqrt{2\pi}\sigma_i} \exp\left[-\frac{(q - q_i)^2}{2\sigma_i^2} \right] \right\} + B \qquad (2)$$

where A_i, σ_i, q_i, and B are the peak area, standard deviation, and q position for the ith peak ($i = 1$ for LAM and $i = 2$ for HEX), and background, respectively. An example of the peak decomposition is shown in Figure 4b for the annealing time of 10 min at 168 °C. From the evaluated peak area of LAM and HEX first-order peak, the fraction of LAM phase in coexisting phases (ϕ_L) is estimated by $\phi_L = A_{LAM}/(A_{LAM} + A_{HEX})$, because of isotropically or randomly oriented polygrain structures for both microphases.

Figure 5 gives temporal changes in ϕ_L vs the annealing time at several T-jump temperatures. It is seen that at temperatures lower than 160 °C the morphological

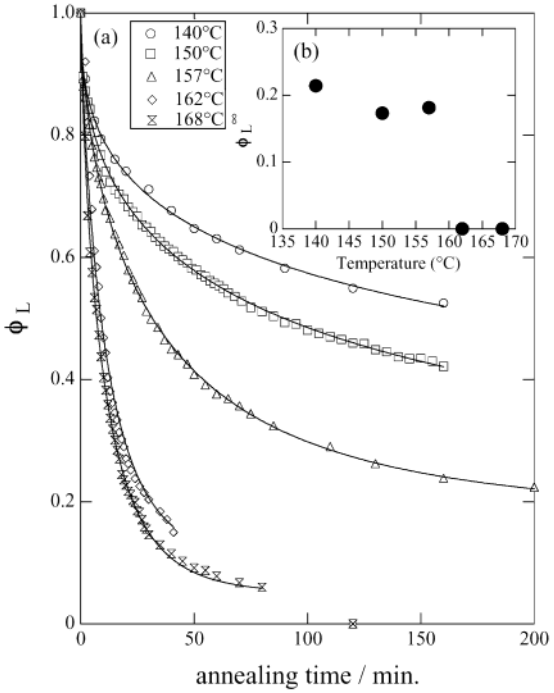

Figure 5. (a) Temporal changes in the amount of LAM phase, ϕ_L. The solid curves are the fitting by the Avrami-type decay function as given by eq 3. (b) Plot of ϕ_L^∞ (the amount of LAM phase at $t = \infty$) vs the annealing temperature. The values were evaluated by the fitting below 157 °C, while they were set as $\phi_L^\infty = 0$, which are directly determined by the SAXS results for 162 and 168 °C.

transition from LAM to HEX was not completed even at prolonged annealing times above 200 min, indicating that the mixture of LAM and HEX phases still exists. But, as the T-jump was elevated (above 162 °C), the transition was more accelerated and the HEX formation seems to be completed within 120 min. The decay of ϕ_L with the annealing time, t, was analyzed by using the Avrami-type decay function

$$\phi_L(t) = (1 - \phi_L^\infty) \exp\{(-t/\tau)^n\} + \phi_L^\infty \qquad (3)$$

where ϕ_L^∞ is the amount of LAM phase at $t = \infty$, τ is a decay time, and n is the Avrami exponent. The curve fittings with adjusting τ, n, and ϕ_L^∞ shown by solid lines in Figure 5 give good agreements with experimental data. The complete transition to the HEX cylinders was attained at $t \geq 120$ min for 162 and 168 °C. Since, the fitting with eq 3 became far from the experimental data at $t = 120$ min, we neglected SAXS data at 120 min for both 162 and 168 °C in the fitting shown in Figure 5. The inset in Figure 5 shows the plot of ϕ_L^∞ vs the annealing temperature, where the values below 157 °C are evaluated by the fitting, while those for 162 and 168 °C are set as $\phi_L^\infty = 0$, which are directly obtained from the SAXS measurements. The behavior of ϕ_L^∞ exhibits a discontinuity around 160 °C.

Figure 6 gives temporal changes of G' for two T-jumps (157 and 168 °C). We also carried out other T-jumps, although the results are not shown here due to the space limit. The temperature profiles for this experiment are shown in the upper panel of Figure 6. At point A, temperature was jumped up from 90 to 110 °C, at B to 168 °C (or 157 °C), and then finally at C from 168 °C (or at C′ from 157 °C) to 110 °C. The duration time at

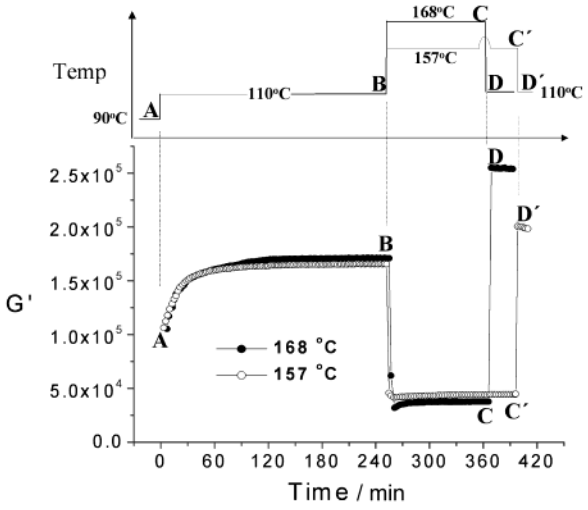

Figure 6. Temporal changes in G' measured at a frequency 0.1 rad/s and a strain of 0.005. Temperature profiles are shown in the upper panel: 157 °C (○); 168 °C (●).

157 °C was longer than that at 168 °C, since the transition of HEX was slower for lower temperatures, as shown in Figure 5.

It is seen that during the first heating from 90 to 110 °C G' increased very rapidly, and then it approached steady value after ca. 60 min. A sharp increase in G' is attributed to the increased perfection of the LAM ordering, as discussed in Figure 1. Because of the T-jump at point B, G' decreased stepwise and then started to increase and approached their asymptotic values. G' at 168 °C starts from a slightly smaller value than that at 157 °C since higher temperature gives smaller G'. But, the increasing rate was faster for the former, suggesting that the transition of HEX was achieved earlier.

Finally, when we quenched from higher temperatures to 110 °C at point C (or C′), G' at point D (or D′) was larger than G' at point B. Also, G' at point D was higher than that at point D′. The microdomain structures at point D after quenching are essentially the same as those at higher temperatures (or point C) because of the immobilization of PS blocks. Therefore, the difference in G' between point D and point B depends on the fraction of LAM phase and macroscopic grain conditions such as size, shape, and number. The reason why G' of HEX microdomains becomes higher than that of LAM is not clear. To the best of our knowledge, there has been no report on the viscoelastic behavior during the direct transition from LAM to HEX. However, it is considered that, within the linear viscoelastic region, the modulus depends mainly upon the interfaces normal to the flow direction[23] and microstructure connectivity.[17,32] The transition from LAM to HEX gives more interfaces; thus, an increase in newly-generated interfaces normal to the flow direction results in larger G'. Similar behavior has been observed for OOTs from HEX to BCC and from LAM to HPL structure.[17−23,28−34]

To examine the dependence of G' on the amount of LAM phase during the OOT, the changes of G'/G_0 with time during the process B → C are magnified in Figure 7a. Here, G_0 is the minimum value of G' during this process, which decreases with increasing temperature. It is seen that with increasing T-jump the value of G'/G_0 increases, and the steady value would be achieved at earlier times. Since we assume that G' of HEX state

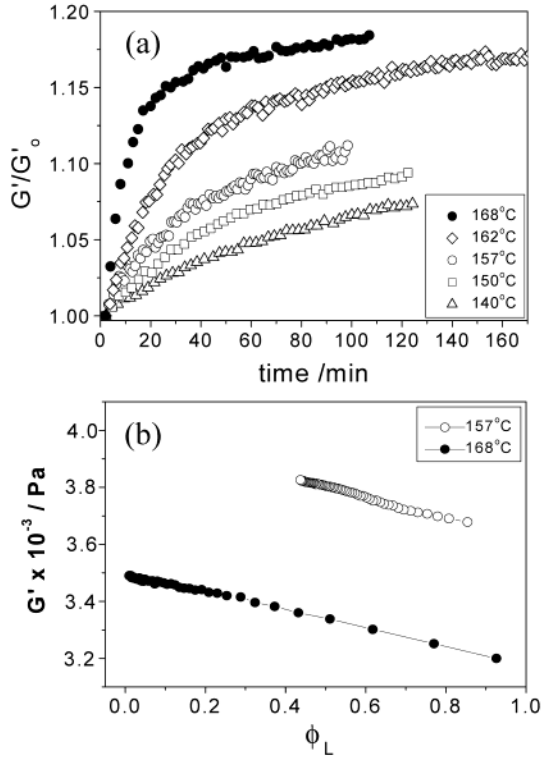

Figure 7. (a) Temporal changes in G'/G_0 at a frequency of 0.1 rad/s during T-jumping from 110 °C to several temperatures: 140 (△), 150 (□), 157 (○), 162 (◇), and 168 °C (●). (b) Plot of G' vs ϕ_L for two T-jumps: 157 (○) and 168 °C (●). The ϕ_L was evaluated independently from the SAXS results:

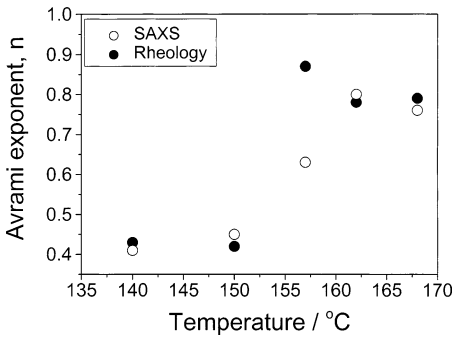

Figure 8. Avrami exponent (n) with the annealing temperature, which is evaluated from SAXS (○) and rheology (●).

is larger than that of LAM state, the value of G'/G_0 is directly related to the amount of HEX phase. Since the amount of HEX (or LAM) phase was already estimated from SAXS experiments (see Figure 5), we plot G' vs ϕ_L at two temperatures, as given in Figure 7b. It is seen that a linear relationship between these two parameters is valid: $G'_{TOTAL} = \phi_L G'_{LAM} + (1 - \phi_L)G'_{HEX}$. Previously, Floudas et al.[25] simply assumed this relationship without showing experimental data. From the results of Figure 7, we conclude that G' linearly increases with increasing amount of HEX phase, and the conversion to HEX phase from LAM phase increases and the steady value is achieved faster with increasing T-jump temperature.

The temperature dependence of the Avrami exponent n can give a primitive idea on the transition mechanism. Figure 8 displays the Avrami exponent n from SAXS experiments (open circle) and rheology (solid circle). The exponents from the two approaches are in good agreement except those of 157 °C T-jump. Quite interestingly,

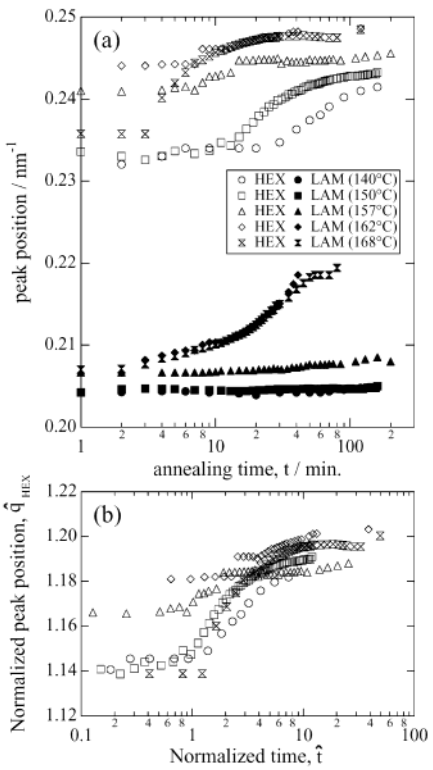

Figure 9. (a) Temporal changes in the SAXS peak positions of LAM and HEX phases during the OOT. (b) Plots of normalized cylinder peak positions ($\hat{q}_{HEX}$) vs normalized annealing time ($\hat{t}$). Here, $\hat{q}_{HEX}$ is defined by q_{HEX} divided by the lamellar peak position (q^0_{LAM}) at $t = 0$ and $\hat{t} = t/t_X$. t_X is defined as an annealing time at which ϕ_L reaches $\phi_{L,crit}$ (=0.73).

n of 140 and 150 °C T-jump is ca. 0.43, whereas n of 162 and 168 °C T-jump is ca. 0.8. According to the Avrami-type crystallization theory,[38,39] the exponent (n) is correlated with the dimensionality of the crystal growth, for instance, 0.5 for one-dimensional growth (rodlike crystallite) and 1.0 for two-dimensional growth (disklike crystallite) when the crystallization is controlled by diffusion of molecules. The discontinuity of the exponents at 160 °C, as shown in Figure 8, suggests different dimensionality of growth of HEX cylinders below and above ca. 160 °C, although OOT is not the same phenomenon as the crystallization where molecules migrate from disordered state to ordered state (crystals).

Peak positions and full width at half-maximum (fwhm) are valuable information on the temperature dependence of the transition mechanism. Temporal changes in the double first-order peak positions are shown in Figure 9a. Below 157 °C, the LAM peak position remains almost constant, while it gradually increases with time above 162 °C. For the temporal change in the HEX peak position, there seems to be a general tendency that peak position remains constant at the early stage, then gradually increases with time, and finally reaches constant. If we define the threshold time (t_X) as an annealing time after which the HEX peak position increases, t_X was found to decrease with increasing the annealing temperature. It was seen from Figures 5 and 9a that the value of ϕ_L at t_X was almost the same (~0.73) irrespective of the annealing temperatures. It is mentioned, however, that the critical value of ϕ_L ($\phi_{L,crit} \sim 0.73$) was experimentally determined without any theoretical argument.

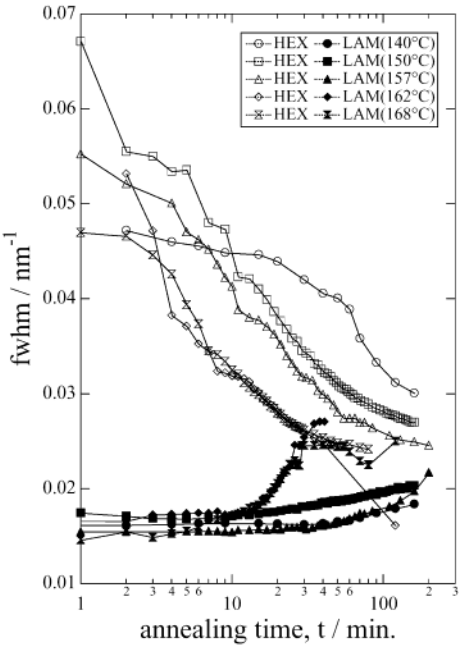

Figure 10. Temporal changes in the full width at half-maximum (fwhm) of double first-order peaks with the annealing time as a function of the annealing temperature.

Figure 9b shows plots of normalized cylinder peak positions ($\hat{q}_{HEX}$) vs normalized annealing time ($\hat{t}$). Here, $\hat{q}_{HEX}$ is defined by q_{HEX} divided by the lamellar peak position (q^0_{LAM}) at $t = 0$, and $\hat{t} = t/t_X$, in which t_X is an annealing time at which ϕ_L reaches $\phi_{L,crit}$. It is seen in Figure 9b that the $\hat{q}_{HEX}$ does not change with time for $\hat{t} \leq 1$, implying that the generation of the HEX cylinders from LAM phase is frustrated by the majority phase of the remaining LAM phase as long as ϕ_L is larger than $\phi_{L,crit}$. On the other hand, as shown in Figure 9a, the LAM first-order peak above 162 °C shifts toward higher q with time after 10 min at which ϕ_L reaches 0.4−0.5 (see Figure 5). Note that the LAM first-order peak below 157 °C does not start to shift even at the same value of ϕ_L (0.4−0.5). This fact indicates that the shift of the LAM first-order peak cannot be accounted for in terms of the change in ϕ_L, as opposed to the shift of the HEX first-order peak. It may be therefore suggested that the morphological change to HEX phase occurring inside the LAM phase at the T-jump below 157 °C is different from that for the T-jump above 162 °C. This result is consistent with the growth mechanism (dimensionality) based on the Avrami exponent n.

The change in fwhm of the double first-order peaks with the annealing time at several temperatures is shown in Figure 10. There seems to be a correlation between the behaviors of fwhm and the peak position. Note that the peak width relates to the degree of regularity of ordered microdomains. Overall, the peak width for the HEX cylinders monotonically decreases with time, indicating improvement of the packing regularity. The only exception is the case of the 140 °C annealing, where the fwhm stayed constant in the early stage below about 20 min, which closely coincides with the behavior of the peak position. As for the LAM phase, the fwhm stays almost constant below 157 °C, while it suddenly increases at ca. 10 min for the annealing temperatures above 162 °C. Namely, the remaining lamellar phase is unaffected by the ongoing transition for the former case, while it is significantly affected for the latter case. These facts again suggest the difference in the transition mechanism between lower and higher temperatures.

Wang et al.[10,11] theoretically showed that the transition from weakly segregated LAM to HEX by T-jump undergoes stepwise processes with modulation and perforation of LAM. For shallow T-jumps where the transition occurs slowly, the initial stage of the HEX evolution is a simple decay of LAM ordering and in-layer density modulation begins to emerge. However, the interlayer correlation of the modulations would not be high, suggesting that in-layer modulation plays a major role. On the contrary, for deep T-jumps where the transition occurs fast, the interlayer correlation of the modulation as well as the in-layer modulation can be effective. This suggests that the remaining LAM is strongly affected by the other in-layer fluctuations, possibly resulting in considerable interlayer correlation. These two transition mechanisms result in difference in the dimensionality of the growth of HEX microdomains, as inferred from the Avrami exponents. Two-dimensional fluctuation, corresponding to the fast transition, may cause perforated structure as an intermediate state with a periodicity of twice the lamellar spacing during LAM to HEX transition, although the detection of this intermediate state depends on its lifetime. On the other hand, in a transition governed by one-dimensional fluctuation corresponding to slow transition, the formation of the intermediate state such as perforated structure is as little as possible. The TEM results in Figure 3 are consistent with different transition mechanisms.

On the basis of the above-mentioned arguments, the possibility to observe an intermediate state (or metastable state) becomes higher as the dimensionality of the fluctuation (or transition rate) increases. Then, we consider that 3-dimensional fluctuation (or spinodal decomposition) might be expected for a very rapid transition, namely a very high annealing temperature, although the detection of an intermediate state by experiments is not easy due to very short lifetime. On the other hand, if an as-cast sample has poor ordering (or regularity) of LAM, the transition to equilibrium HEX state becomes very rapid. This kind of very rapid transition might be achieved if the mismatch of the lattice spacing between LAM in an as-cast sample and equilibrium HEX is small. In these two cases, the transition from nonequilibrium LAM to equilibrium HEX takes place via spinodal-like fluctuation, giving an intermediate state (or metastable state).[9] The validity of this scenario is currently under investigation. It should be mentioned that the existence of an intermediate state is also dependent upon volume fraction of minor block (ϕ_{PS}). As the difference between ϕ_{PS} and a volume fraction at which PL (or ML) structure is expected is smaller, the possibility of the appearance of PL (or ML) becomes higher during the transition from nonequilibrium LAM to equilibrium HEX. The volume fraction of ϕ_{PS} in SEBS studied here was 0.23, which was smaller than that ($\phi_{PS} = 0.3-0.35$) in refs 28−30 where an intermediate state was confirmed.

Finally, we evaluated the apparent activation energies for the morphological transitions based on the temperature dependence of the decay time, τ, which are obtained from SAXS and rheology. Figure 11 gives the Arrhenius plot of the decay rate, τ^{-1}, vs the inverse of the absolute temperature. The apparent activation

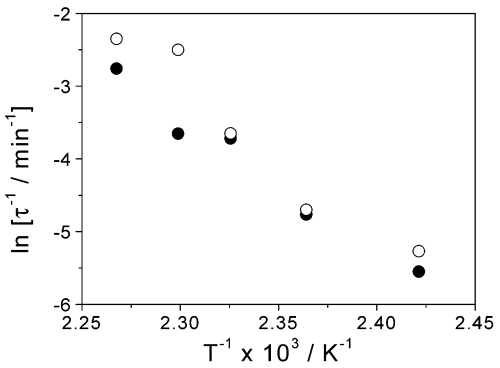

Figure 11. Arrhenius plots, ln τ^{-1} vs inverse of the absolute temperature, evaluated from SAXS (○) and rheology (●).

energy obtained from SAXS (open circle) is 42 kcal/mol, which is close to that (36 kcal/mol) from rheology (solid circle). Interestingly, this value is quite close to that of the transition from nonequilibrium PB cylinders to equilibrium PS−PB lamellae in SBS triblock copolymers (ca. 40 kcal/mol) studied previously.[14] Furthermore, this value is close to that (38 kcal/mol) of PS homopolymer in the relevant temperature ranges but much larger than that (4.8 kcal/mol) of neat polybutadiene or PEB.

Since the rate of the OOT, however, is determined by the degree of regularity and orientation of microdomains,[30] it is reasonable to compare the activation energy for other OOTs. Floudas et al.[25] have reported similar values of the activation energy (ca. 47 kcal/mol) for epitaxial OOT from cylinder to gyroid in polyisoprene-*block*-poly(ethylene oxide) copolymers based on the SAXS results. They also found ca. 60 kcal/mol from rheological measurement with a small strain (γ_0 = 0.005). Note that these values are much higher than that of polyisoprene and poly(ethylene oxide) local segmental relaxation (typically 5−10 kcal/mol at $T - T_g = 220$ K). They argued that the OOT was controlled by a collective motion associated with the bicontinuous cubic phase (gyroid). This argument is also applied to the OOT studied in this study. For instance, even though the activation energy for OOT in the SBS studied previously (from HEX to LAM) and that in the present SEBS case (from LAM to HEX) was similar, the transition for the SEBS was much slower. For instance, the SBS exhibited complete transformation from HEX to LAM after 170 min annealing even at 127 °C, whereas for SEBS a slight transition to HEX from LAM is expected at 127 °C even at very prolonged annealing time (maybe over 180 min). This also shows that the collective motion of the interface plays a main role in the transition; that is, OOT in this study is controlled by the segregation power and the degree of perfection (or regularity) of microdomain structure rather than the motions of PS block chains themselves.

IV. Conclusions

In this study, we have shown, via time-resolved SAXS, TEM, and rheology, that a nonequilibrium LAM microdomains formed during toluene casting was transformed into HEX microdomains at higher temperatures. During this transition, the coexistence of the LAM and HEX microdomains was clearly observed during the entire process of OOT from LAM to HEX, and the lamellar fraction in the coexisting phase decreased with annealing time. Even though a small portion of the intermediate structure of PL (or ML) was observed only at higher annealing temperatures, which was confirmed by TEM, we did not find a clear evidence of this intermediate structure by SAXS and rheology.

We have also shown that the G' of the HEX phase was larger than that of the LAM phase and that G' increased linearly with the amount of HEX phase in coexisting phases. The Avrami exponent (n) at higher annealing temperatures (above 160 °C) was larger than that at lower annealing temperatures. Thus, at lower temperatures, one-dimensional growth from the in-layer modulation induced the nucleation and growth of HEX microdomains, but at higher temperatures the nucleation and growth resulted from both interlayer correlation of the modulation and in-layer modulation of LAM layers (2-dimensional growth).

Acknowledgment. This work was supported by the Korean-Japan joint Research program (986-0300-004-2) supported by KOSEF and JSPS and by Applied Rheology Center governed by KOSEF. Synchrotron SAXS at the PLS (4C1 beamlines) was supported by the Ministry of Science and Technology (MOST) and Pohang Iron and Steel Co. (POSCO). The financial support by Grant-in-Aid from Japan Ministry of Education, Science, Culture, and Sports with 08751048 granted to S.S. is also gratefully acknowledged.

References and Notes

(1) Molau, G. E. In *Block Polymers*; Aggarwal, S. L., Ed.; Plenum Press: New York, 1970.
(2) Bates, F. S.; Fredrickson, F. S. *Annu. Rev. Phys. Chem.* **1990**, *41*, 265.
(3) Leibler, L. *Macromolecules* **1980**, *13*, 1602.
(4) Matsen, M. W.; Bates, F. S. *Macromolecules* **1996**, *29*, 1091.
(5) Holden, G., Legge, N. R., Quirk, R., Schroeder, H. E., Eds.; *Thermoplastic Elastomers*, 2nd ed.; Hanser: Munich, 1996.
(6) Goveras, J. L.; Milner, S. T. *Macromolecules* **1977**, *30*, 2605.
(7) Matsen, M. W.; Schick, M. *Phys. Rev. Lett.* **1994**, *72*, 2660.
(8) Matsen, M. W. *Phys. Rev. Lett.* **1998**, *80*, 4470.
(9) Laradji, M.; Shi, A.-C.; Desai, R. C.; Noolandi, J. *Phys. Rev. Lett.* **1997**, *78*, 2588; *Macromolecules* **1997**, *30*, 3242.
(10) Qi, S.; Wang, Z.-G. *Phys. Rev. Lett.* **1996**, *76*, 1679; *Phys. Rev. E* **1997**, *55*, 1682.
(11) Qi, S.; Wang, Z.-G. *Macromolecules* **1997**, *30*, 4491; *Polymer* **1998**, *39*, 4439.
(12) Sakurai, S.; Momii, T.; Taie, K.; Shibayama, M.; Nomura, S.; Hashimoto, T. *Macromolecules* **1993**, *26*, 485.
(13) Sakurai, S.; Hashimoto, T.; Fetters, L. J. *Macromolecules* **1996**, *29*, 740.
(14) Sakurai, S.; Umeda, H.; Taie, K.; Nomura, S. *J. Chem. Phys.* **1996**, *105*, 8902.
(15) Sakurai, S.; Umeda, H.; Furukawa, C.; Irie, H.; Nomura, S.; Lee, H. H.; Kim, J. K. *J. Chem. Phys.* **1998**, *108*, 4333.
(16) Sakurai, S.; Irie, H.; Umeda, H.; Nomura, S.; Lee, H. H.; Kim, J. K. *Macromolecules* **1998**, *31*, 336.
(17) Khandpur, A. K.; Förster, S.; Bates, F. S.; Hamley, I. W.; Ryan, A. J.; Bras, W.; Almdal, K.; Mortensen, K. *Macromolecules* **1995**, *28*, 8796.
(18) Koppi, K. A.; Tirell, M.; Bates, F. S.; Almdal, K.; Mortensen, K. *J. Rheol.* **1994**, *38*, 994.
(19) Hajduk, D. A.; Takenouchi, H.; Hillmyer, M. A.; Bates, F. S.; Vigild, M. E.; Almdal, K. *Macromolecules* **1997**, *30*, 3788.
(20) Kim, J. K.; Lee, H. H.; Ree, M.; Lee, K.-B.; Park, Y. *Macromol. Chem. Phys.* **1998**, *199*, 641.
(21) Kim, J. K.; Lee, H. H.; Gu, Q.; Chang, T.; Jeong, Y. H. *Macromolecules* **1998**, *31*, 4045.
(22) Sakamoto, N.; Hashimoto, T.; Han, C. D.; Kim, D.; Vaidya, N. Y. *Macromolecules* **1997**, *30*, 1621.
(23) Ryu, C. Y.; Lee, M. S.; Hajduk, D. A.; Lodge, T. *J. Polym. Sci., Polym. Phys. Ed.* **1997**, *35*, 2811.
(24) Gido, S. P.; Wang, Z.-G. *Macromolecules* **1997**, *30*, 677.
(25) Floudas, G.; Ulrich, R.; Wiesner, U. *J. Chem. Phys.* **1999**, *110*, 652.
(26) Sakurai, S. *Curr. Trends Polym. Sci.* **1996**, *1*, 119.
(27) Ryu, C. Y.; Vigild, M. E.; Lodge, T. P. *Phys. Rev. Lett.* **1998**, *81*, 5354.

(28) Hamley, I. W.; Koppi, K. A.; Rosedale, J. H.; Bates, F. S.; Almdal, K.; Mortensen, K. *Macromolecules* **1993**, *26*, 5959.
(29) Hajduk, D. A.; Gruner, S. M.; Rangarajan, P.; Register, R. A.; Fetters, L. J.; Honeker, C.; Albalak, R. J.; Thomas, E. L. *Macromolecules* **1994**, *27*, 490.
(30) Wang, C.-Y.; Lodge, T. P. *Macromol. Rapid Commun.* **2002**, *23*, 49; *Macromolecules* **2002**, *35*, 6997.
(31) Schulz, M. F.; Bates, F. S.; Almdal, K.; Mortensen, K. *Phys. Rev. Lett.* **1994**, *73*, 86.
(32) Zhao, J.; Majumdar; B.; Schulz, M. F.; Bates, F. S.; Almdal, K.; Mortensen, K.; Hajduk, D. A.; Gruner, M. F. *Macromolecules* **1996**, *29*, 1204.
(33) Forster, S.; Khandpur, A. K.; Zhao, J.; Bates, F. S.; Hamley, I. W.; Ryan, A. J.; Bras, W. *Macromolecules* **1994**, *27*, 6922.
(34) Ahn, J. H.; Zin, W. C. *Macromolecules* **2000**, *33*, 641.
(35) Krishnamoorti, R.; Modi, M. A.; Tse, M. F.; Wang, H. C. *Macromolecules* **2000**, *33*, 3810.
(36) Grulke, E. A. In *Polymer Handbook*, 3rd ed.; Brandrap, J., Immergut, E. H., Eds.; Wiley: New York, 1989.
(37) Hashimoto, T.; Kawamura, T.; Harada, M.; Tanaka, H. *Macromolecules* **1994**, *27*, 3063.
(38) Avrami, M. J. *J. Chem. Phys.* **1939**, *7*, 1103.
(39) Schultz. J. M. *Polymer Crystallization-The Development of Crystalline Order in Thermoplastic Polymers*; Oxford University Press: New York, 2001.

MA021376V